https://doi.org/10.1016/j.renene.2019.08.122

This is the Pre-Published Version.

Numerical investigation of the average wind speed of a single wind turbine and development of a novel three-dimensional multiple wind turbine wake model

Haiying Sun*, Hongxing Yang

Renewable Energy Research Group (RERG), Department of Building Services Engineering,
The Hong Kong Polytechnic University, Hong Kong, China

Abstract

This paper reports the newly developed three-dimensional analytical wake models for single and multiple wind turbines. Firstly, the average wind speed of a single wind turbine is studied based on the single wake model. For a single wind turbine, assuming the incoming wind is distributed as power law in the vertical direction, the average wind speeds have a close relationship to the power exponent α , the hub height h_0 and the rotor radius r_0 . When $\alpha = 0.4$, the average wind speed can decrease to 96% of the speed at the hub height. Secondly, the three-dimensional multiple wake model is developed based on the single wake model. The method of Sum of Squares is applied to solve the wake adding problem. The available wind tunnel experimental data of two different layouts are used to validate the wake model. At the three representative heights, the wake model predicts the distribution of wind speed accurately. For Layout 1, at the hub and the top heights, most of the relative errors between the wake model results and the experimental data are smaller than 6%. At the top height, all relative errors are smaller than 20%. For Layout 2, the largest errors of the wake model are 8.5% at the top height, 17.8% at the bottom height and 21.2% at the hub height. The results predicted by the multiple wake model are demonstrated as well. The presented wake model can be used to describe the wind distribution and optimize the layout of wind farm.

Keywords: Average wind speed; Three-dimensional multiple wake model; Validation by wind tunnel experiments; Wake distribution prediction.

1. Introduction

For horizontal wind turbines, wake models can be categorized into analytical models [1] and numerical wake models [2]. In view of optimizing the wind turbine (WT) locations, numerical models tend to be more precise, but analytical models have more advantages because of their simplicity and fast computational speed [3].

When optimizing wind farms, the one-dimensional (1-D) wake model proposed by Jensen [4] is the most widely used one. The assumptions of Jensen wake model are quite simple but obviously unrealistic. The wind speed is regarded as a constant in the wake influenced area at a specific downwind distance, and it is assumed to be identical in different radial positions. Some scholars then proposed more accurate models based on Jensen wake model, but the models are more complicated. Ishihara, et al. [3] considered how turbulence affects the rate of wake recovery and they developed a universal wake model. The wake can be predicted by the proposed model for any thrust coefficient and ambient turbulence. Larsen [5] presented a semi-analytical algorithm for computation of stationary wind fields. The model considers wakes as linear perturbations on the ambient non-uniform mean wind field. Although they considered other factors in the following models, the simplification models were only constrained for flat terrains. Kuo, et al. [6] proposed a numerical wake model to simulate wake effects over complex terrains. It implemented simplifications and assumptions to solve a simplified variation of the Navier-Stokes equations. However, this model was not applied to the multiple wake effect. Song, et al. [7] simulated the turbulence of WT's wake flow and the effect of velocity decay as well. They decoupled the wake flow solution from the wind speed field. The wake model regarded the wake intensity as a diffusive and

* Corresponding author. Tel.: 2766 4815
E-mail address: haiying.sun@connect.polyu.hk

© 2019. This manuscript version is made available under the CC-BY-NC-ND 4.0 license https://creativecommons.org/licenses/by-nc-nd/4.0/.

convective virtual matter. The model can predict the turbulence of wake and the distribution of wind speed decay in the complex terrain with a non-uniform flow field.

Recently, some wake models were developed based on new findings about wake characteristics. Chamorro and Porté-Agel [8] conducted research on the wind deficit behind a single WT with the wind tunnel experiments, whereas Dufresne and Wosnik [9] investigated the traditional shear flow theories in wakes. Both experimental and theoretical investigations drew the conclusion that beyond a distance downstream of a WT, the shape of wind speed deficit is similar to Gaussian axisymmetric. Based on these findings, the 1-D wake models were further developed. In recent years, inspired by Jensen wake model, certain two-dimensional (2-D) WT wake models were developed. In 2014, Bastankhah and Porté-Agel [10] established a wake model, which was validated by experimental case studies and an Large Eddy Simulation (LES) method. Although three variables were involved in the wake model, only two of them influenced the wind distribution, which were the downwind distance and the distance to the hub axis. Tian, et al. [11] proposed the Cosine wake model in 2015, in their model, the shape of wind speed profile on the horizontal level was cosine form. In 2016, Gao, et al. [12] developed the Jensen-Gaussian 2-D wake model, of which the assumption was that the shape of wind speed is Gaussian-shaped in the horizontal direction. The authors of this study have previously presented and validated an analytical three-dimensional (3-D) wake model for single WT [13]. The proposed model is more realistic and more precise, because it also considers the wind variation in the vertical direction. The basic theory of the 3-D wake model is the flow flux conservation law. It assumes that the deficit of wind speed is Gaussian-shaped within a downwind wake-influenced section. The model has been proved to be accurate in predicting the distribution of wind speed in spatial and it has the potential to optimize the layouts of nonuniform wind farms [14].

On the other hand, to conduct the detailed numerical simulation, some researchers applied Computational Fluid Dynamics (CFD) methods and took experiments of WT wake flow, especially in the fluid mechanics field. They tried to better understand the nature and the interaction of multiple wake flows. Jimenez, et al. [15] programmed a CFD code based on LES approach. Concentrated drag forces were applied to simulate WTs, which were fixed in anisotropy turbulence. The results were in good agreement with analytical correlations and experimental data. Wu and Porté-Agel [16] also used LES to study the characteristics of WT wake in a flow of neutral turbulent boundary-layer. The simulation results were validated by the high-resolution measuring data from a hot-wire anemometry behind the miniature WT. Yang and Sotiropoulos [17] validated an LES-actuator disk model by wind tunnel measurements. For the case of single WT, good agreement was obtained between the model simulations and the tested data at far downstream locations, discrepancies existed in the near wake zone. For the wind farm case, perfect downwind results were obtained at both bottom and top tip heights. Some discrepancies were at the hub height of WTs. Sedaghatizadeh, et al. [18] developed a fully numerical wake model by LES. The LES model was more accurate compared to the semi-empirical wake models that were commonly applied in the industry. It was also used as a benchmark to compare the accuracy of those semi-empirical models. Chamorro, et al. [19] studied the basic properties of wake flow in a staggered wind farm through wind tunnel tests. The staggered configuration was more efficient than the aligned layout in both streamwise and spanwise directions. The maximum turbulence intensity level of the staggered configuration was similar to that of a single WT, but it was substantially different from that of the aligned layout with a similar spacing. Tian, et al. [20] conducted an experiment and found that the discrepancies from the upper-stream wind could significantly influence the characteristics of wake and the loads on the WT model. The formation, shedding and breakdown of different unstable wake vortices were found to determine the flow characteristics of the WT wake. Wildmann, et al. [21] used long-range lidar instruments to detect and analyze the wake of a single WT in the complex terrain. A wake tracking algorithm was proposed to detect the wake center in the lidar scans for three periods with distinct atmospheric stability conditions.

Data from wind tunnel and wind field experiments are useful for wake studies, however, it is not practical to solve wind farm layout problems through those studies. Full CFD is accurate in describing wind flow, but applying it in the wind farm design process is difficult. When optimizing the positions of WTs, all optimization algorithms require numerous times of calculation for the wake flow, because there is a huge quantity of various layouts of wind farms. Time cost on evaluating wake distributions of various layouts with multiple WTs is even more unacceptable.

In this paper, the 3-D single WT wake model developed by authors of this study before is further investigated. In chapter 2, the average wind speed of single WT is investigated based on the inflow profile adopted in the 3-D single wake model. The equation is derivated firstly, and then the analysis is shown under four wind speed power law parameters. In chapter 3, the derivation of the 3-D multiple WT wake model is demonstrated step by step. In chapter 4, the validation of the 3-D multiple wake model is conducted by comparing to the available wind tunnel experimental data with two different layouts. In chapter 5, the predictions from the 3-D multiple wake model are demonstrated. In chapter 6, the main information of this paper is summarized.

Nomenclature

List of abbreviations		r	radial distance to the centerline (m)
1-D	one-dimensional	r_0	rotor radius of wind turbine (m)
2-D	two-dimensional	$r_w(x)$	wake-influenced radius (m)
3-D	three-dimensional	$S_{r_w(x)}$	circular area with radius $r_w(x)$ (m^2)
CFD	Computational Fluid Dynamics	S_{r_0}	circular area with radius r_0 (m^2)
D	the rotor diameter of the wind turbine	u_0	wind velocity at z_r height (m/s)
LES	Large Eddy Simulation	u_{h0}	the wind speed at the hub height (m/s)
WT	wind turbine	$U(x)$	wind velocity in 1-D wake model (m/s)
		$U(x,r)$	wind velocity in 2-D wake model (m/s)
List of symbols		$U(x,y,z)$	wind velocity in 3-D wake model (m/s)
a	factor of axial induction	$U_0(z)$	incoming wind speed distribution (m/s)
$A(x)$	parameter in 3-D wake model (m^2)	v_0	average wind speed behind wind turbine (m/s)
$B(x)$	parameter in 3-D wake model (m/s)	z_0	roughness length of aerodynamic surface (m)
C	parameter in 3-D wake model	z_r	reference height (m)
h_0	hub height of wind turbine (m)	α	parameter in wind speed power law
k_{wake}	wake decay constant	$\sigma(x)$	parameter in 3-D wake model (m)
$Q(x)$	total flow flux (m^3/s)		

2. Average wind speed of the three-dimensional wake model

2.1 Introduction of the three-dimensional wake model

A 3-D single WT wake model was presented by Sun and Yang [13] as follows,

$$U(x,y,z) = A(x)\left(\frac{1}{2\pi\sigma(x)^2} e^{-\frac{y^2+(z-h_0)^2}{2\sigma(x)^2}}\right) + B(x) + U_0(z) \tag{1}$$

In equation (1), h_0 is the height of the WT hub. $A(x)$, $B(x)$, and $\sigma(x)$ are the significant parameters that determine the Gaussian-shaped deficits of wind speeds. For the sake of simplifying the process of calculation, $\sigma(x)$ is determined by $\sigma(x) = \frac{r_w(x)}{C}$. $r_w(x)$ is the wake-influenced radius, and C is a constant, which is to be determined based on real operating conditions. $A(x)$ and $B(x)$ can be represented by C, as shown in equation (2).

$$\begin{cases} A(x) = \dfrac{Q(x) - \int_{h_0 - r_w(x)}^{h_0 + r_w(x)} 2\sqrt{r_w(x)^2 - (z - h_0)^2}\, U_0(z)dz}{\left(1 - e^{-\frac{C^2}{2}} - \frac{C^2}{2} e^{-\frac{C^2}{2}}\right)} \\ B(x) = -\dfrac{A(x)C^2}{2\pi r_w(x)^2} e^{-\frac{C^2}{2}} \end{cases} \tag{2}$$

$Q(x)$ is the total flow flux, which is obtained from equation (3).

$$Q(x) = \pi r_0^2 v_0 + \iint\limits_{S_{r_{wj}(x)} - S_{r_0}} U_0(z) ds \tag{3}$$

$U_0(z)$ is the distribution of the incoming wind speed, and it is denoted by equation (4). The power wind distribution is widely used [14, 22, 23], details about which can be found in reference [24].

$$U_0(z) = u_0 \left(\frac{z}{z_r}\right)^{\alpha} \tag{4}$$

In the equation, z_r is the height of reference, u_0 is the wind speed measured at z_r, and α is the parameter of wind speed power law. α and z_r can be obtained from Table 1.

Table 1 Parameter of wind speed power law [22, 25]

The type of terrain	α	z_r (m)
Ocean, lake and smooth hard ground	0.10	200
Open terrain with few obstacles	0.16	250
Terrain uniformly covered by obstacles	0.28	400
Terrain with large irregular objects	0.40	500

2.2 Average wind speed

In the 3-D wake model, the distribution of wind velocity varies at different spatial positions. Therefore, the wind speed at the WT hub height is different from the average wind speed of the WT. To evaluate the energy output of WTs more precisely, the analytical average wind speed is derived in this section.

Supposing u_{h0} is the wind speed at the hub height of the WT. With the power law, u_{h0} can be expressed as equation (5).

$$u_{h0} = u_0 \left(\frac{h_0}{z_r}\right)^{\alpha} \tag{5}$$

u_a is the average wind speed on a WT. The flow flux is conservative within a certain area at the downstream wake section. In the swept area of a WT, S_{r_0} is the circular area, of which the center is at the hub position and the radius is r_0. The flow flux conservation theory is expressed by equation (6):

$$\pi r_0^2 u_a = \iint\limits_{S_{r_0}} U_0(z) ds \tag{6}$$

Then, applying the power law into the above equation, u_a can be solved by equation (7).

$$u_a = \frac{1}{\pi r_0^2} \iint\limits_{S_{r_0}} u_0 \left(\frac{z}{z_r}\right)^{\alpha} ds \tag{7}$$

MATLAB software is applied as the calculation tool in this study. The ratio of average wind speed and the hub height wind speed is studied. With equations (5) and (7), the ratio $\frac{u_a}{u_{h0}}$ can be calculated from equation (8).

$$\frac{u_a}{u_{h0}} = \frac{1}{\pi r_0^2} \iint_{S_{r_0}} \left(\frac{z}{h_0} \right)^{\alpha} ds \tag{8}$$

Figure 1 demonstrates the ratio of average wind speeds and the hub height wind speeds with a series of rotor radii at different hub heights. Four typical values of α are chosen. The results of five rotor radii from 40 m to 120 m are compared. The hub height range is from 60 m to 130 m.

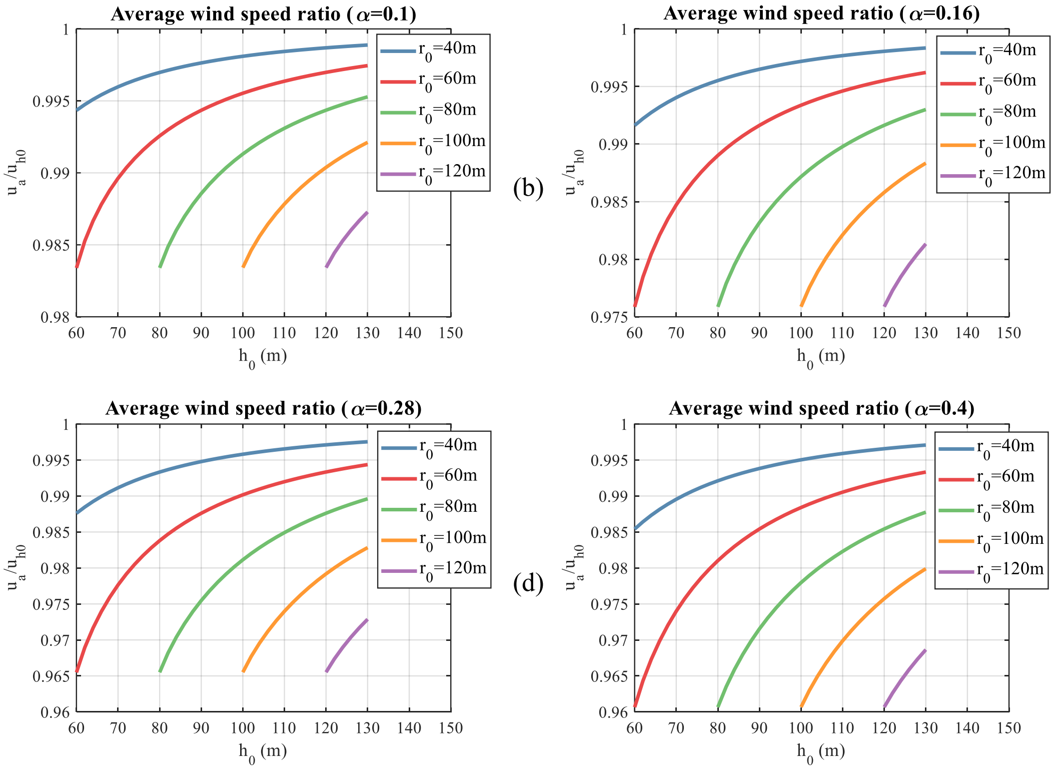

Figure 1 Average wind speed with different values of α : (a) $\alpha = 0.1$; (b) $\alpha = 0.16$; (c) $\alpha = 0.28$; (d) $\alpha = 0.4$.

From the results, the conclusion can be drawn that under the condition of power law distributed incoming wind, the average wind speed of a WT tends to be smaller than that at the hub height. For the same power exponent α, the average wind speed increases with the hub height, but decreases with the rotor radius. For a particular hub height, the average wind speed of $r_0 = 40m$ is successively higher than those of $r_0 = 60m$, $r_0 = 80m$, $r_0 = 100m$, $r_0 = 120m$. For a particular rotor radius, the average wind speed increases gradually from $h_0 = 60m$ to $h_0 = 130m$. The power exponent α also influences the average wind speed. When $\alpha = 0.1$, the average wind speed reduces by 2% to the most, and the reduction raises with the increase of α. When $\alpha = 0.4$, the average wind speed can decrease to 96%. To sum up, the reduction of average wind speed should be considered especially when the rotor has large radius, WTs are fixed at high positions and large irregular objects exist on the wind farm terrains.

3. Derivation of the three-dimensional multiple wake model

In a real wind farm, a WT may be affected by several other WTs' wake effect, thus the study on the 3-D wake model should not only be limited to single wake distribution, but also be extend to multiple wakes. Therefore, a new 3-D multiple wake model is derivated in this section.

3.1 The three-dimensional wake model in a global coordinate

Based on equation (1), the 3-D single wake model can be rewritten based on a global coordinate. For the WT_j at the position of $\left(x_j, y_j\right)$, the wake induced wind distribution $U_j(x,y,z)$ is shown as equation (9):

$$U_j(x,y,z)=\begin{cases} A_j\left(x\right)\left(\dfrac{1}{2\pi\sigma_j\left(x\right)^2}e^{-\frac{\left(y-y_j\right)^2+\left(z-h_0\right)^2}{2\sigma_j\left(x\right)^2}}\right)+B_j\left(x\right)+U_0(z) & \text{, within wake region} \\ U_0(z) & \text{, out of wake region} \end{cases} \tag{9}$$

The wake region is determined by $r_{w_j}\left(x\right)$, which is the radius of the wake influenced circular area at the downwind distance x. If $\left(y-y_j\right)^2+\left(z-h_0\right)^2 \le r_{w_j}\left(x\right)^2$, the point of (x,y,z) is within the wake region. The equation means that the distance from the (x,y,z) point to the hub axis is smaller than the radius of the wake influenced circular area. By contrast, if $\left(y-y_j\right)^2+\left(z-h_0\right)^2 > r_{w_j}\left(x\right)^2$, the point of (x,y,z) is out of the wake region. The equation means that the distance from the point of (x,y,z) to the hub axis is larger than the radius of the wake affected circular area. In the formula, $r_{w_j}\left(x\right)$ can be calculated according to $r_{w_j}\left(x\right)=r_0+k_{wake}(x-x_j)$. Other details about the 3-D single wake model have been described in reference [13].

For the WT_i, which is at the position of $\left(x_i, y_i\right)$ and has the hub height of h_i, if it is under WT_j 's wake effect, the wind speed at WT_i is $U_{ij}(y,z)$, as shown by equation (10):

$$U_{ij}(y,z)=\begin{cases} A_j\left(x_i\right)\left(\dfrac{1}{2\pi\sigma_j\left(x_i\right)^2}e^{-\frac{\left(y-y_j\right)^2+\left(z-h_i\right)^2}{2\sigma_j\left(x_i\right)^2}}\right)+B_j\left(x_i\right)+U_0(z) & \text{, within wake region} \\ U_0(z) & \text{, out of wake region} \end{cases} \tag{10}$$

The two important parameters $A_j\left(x_i\right)$ and $B_j\left(x_i\right)$ are solved by equation (11):

$$\begin{cases} A_j\left(x_i\right)=\dfrac{Q_j\left(x_i\right)-\int_{h_i-r_{w_j}\left(x_i\right)}^{h_i+r_{w_j}\left(x_i\right)}2\sqrt{r_{w_j}\left(x_i\right)^2-\left(z-h_i\right)^2}\,U_0(z)dz}{\left(1-e^{-\frac{C^2}{2}}-\dfrac{C^2}{2}e^{-\frac{C^2}{2}}\right)} \\ B_j\left(x_i\right)=-\dfrac{A_j\left(x_i\right)C^2}{2\pi r_{w_j}\left(x_i\right)^2}e^{-\frac{C^2}{2}} \end{cases} \tag{11}$$

3.2 Wake addition

For the addition of multiple wakes, several methods can be used [26]: Geometric Sum, Linear Superposition, Energy Balance and Sum of Squares. The equations belonging to these models are demonstrated in Table 2.

Table 2 Methods of multiple wake addition [27]

Method	Equation
Geometric Sum	$\dfrac{u_i}{U_\infty}=\prod_j \dfrac{u_{ij}}{u_j}$
Linear Superposition	$(1-\dfrac{u_i}{U_\infty})=\sum_j(1-\dfrac{u_{ij}}{u_j})$

Energy Balance	$U_\infty{}^2 - u_i^2 = \sum_j (u_j{}^2 - u_{ij}{}^2)$
Sum of Squares	$(1-\frac{u_i}{U_\infty})^2 = \sum_j (1-\frac{u_{ij}}{u_j})^2$

u_i is the wind speed of WT_i, u_{ij} is the wind speed of WT_i under the influence of the WT_j 's wake.

A comparative study of four wake models has been conducted with wind tunnel data from GH, i.e. the documentation of WindFarm software [28]. In the comparison, the Sum of Squares method was found excellent for almost all the situations. The next one was the Energy Balance method. Furthermore, it was also recommended that the methods of Linear Superposition and Geometric Sum should not be applied, because they tended to make overestimation on the deficit of wind velocity [27].

In this study, the method of the Sum of Squares is adopted to solve the wake adding problem accordingly. A modification of the Sum of Squares and the method to estimate the average wind speed are combined. To calculate the mean wind speed over the swept area, the deficit of momentum is averaged on area [29]. If WT_i is only under the wake effect of WT_j, equation (12) is adopted. Similarly, u_{a_i} is the average wind speed of WT_i.

$$(u_0 - u_{a_i})^2 = \frac{1}{A}\iint_{S_{r_0}} \left(u_0 - u_{ij}\right)^2 ds \tag{12}$$

The wind speed affected by several wakes on the swept area is calculated by cumulating all momentum deficits of incoming winds and then integrating them, as shown in equation (13).

$$(u_0 - u_{a_i})^2 = \frac{1}{A}\iint_{S_{r_0}} \sum_{j=1}^{\text{all wakes}} \left(u_{a_j} - u_{ij}\right)^2 ds \tag{13}$$

In the above equation, the momentum deficit of the incoming wind is determined as the square of the difference value between the average incoming wind speed and the in-wake wind speed.

u_{a_i} considers all wakes the swept area. With u_{a_i}, the power output of WT_i can be calculated according to the power curve.

3.3 The three-dimensional multiple wake model

Applying the 3-D single wake model [1] to estimate the flow speed in the wake, the method of Sum of Squares is rewritten by equation (14).

$$[1-\frac{U_i(x,y,z)}{U_0(z)}]^2 = \sum_{j=1}^{N}[1-\frac{U_{ij}(y,z)}{U_j(x,y,z)}]^2 \tag{14}$$

Next, with the Sum of Squares, the same modification to equation (12) is made. The variant equation (15) is shown as follows.

$$[U_0(z)-U_i(x,y,z)]^2 = \sum_{j=1}^{N}[U_0(z)-U_{ij}(y,z)]^2 \tag{15}$$

Therefore, the wind distribution of the WT_i can be expressed by equation (16).

$$U_i(x,y,z) = U_0(z) - \sqrt{\sum_{j=1}^{N}[U_0(z)-U_{ij}(y,z)]^2} \tag{16}$$

If WT_i is affected by the wake effect of a number of n WTs, the formula can be further specified by equation (17).

$$U_i(x,y,z)=U_0(z)-\sqrt{\sum_{j=1}^{n}[A_j(x)(\frac{1}{2\pi\sigma_j(x)^2}e^{-\frac{(y-y_j)^2+(z-h_0)^2}{2\sigma_j(x)^2}})+B_j(x)]^2} \tag{17}$$

The average wind speed u_a can be calculated by equation (18).

$$\iint_{S_{r_w(x)}}[U_0(z)-u_a]^2 ds=\iint_{S_{r_w(x)}}[U_0(z)-U(x,y,z)]^2 ds \tag{18}$$

To simplify the calculation, the incoming wind speed $U_0(z)$ on the left side of the equation can be replaced by u_0, therefore the simplified equation (19) is shown as follows.

$$(u_0-u_a)^2=\frac{1}{A}\iint_{S_{r_0}}\sum_{i=1}^{N}[U_0(z)-U(x,y,z)]^2 ds \tag{19}$$

4. Validation of the three-dimensional multiple wake model

To validate the accuracy of the 3-D multiple wake model, the simulations of the wake model are compared to the measured data of the wind tunnel experiment. The experimental data come from the wind tunnel in the Saint Anthony Falls Laboratory at the University of Minnesota, and the experimental conditions are thermally unstratified [30]. Two different layouts of the staggered array of miniature WTs are demonstrated.

4.1 Description of the wind tunnel experiments

The boundary-layer applied to the wind farm model was under neutrally-stratified conditions and grew over a smooth surface. The plan length of the wind tunnel is 37.5 m, the primary fetch of the test section is around 16 m, whereas the cross section size is 1.7 m × 1.7 m. The scale ratio of the area was 6.6:1. More descriptions about the wind tunnel can be found in references [31] and [32].

The intensity of turbulence in the center, i.e. freestream, of the wind tunnel was around 1% for a freestream speed of 2.5 m/s. A turbulent boundary layer depth was obtained with $\delta \approx 0.5m$ at the location of WT. The gradient boundary layer was zero pressure, it had a Reynolds number, $\mathrm{Re}_\delta = U_\infty \delta / \nu \approx 1.12\times10^5$. δ is the boundary layer height.

The friction velocity u_* was 0.13 m/s. The roughness length of aerodynamic surface z_0 was 0.05 mm. u_* and z_0 were acquired by adjusting the profile of the wind velocity to the experimental mean speed in the surface layer.

The WT model consisted of a three-blade GWS/EP-6030 × 3 rotor, which was linked to a tiny DC generator. The WT angular speed was controlled by altering the generator resistance. The dimensions of the WT model are shown in Figure 2.

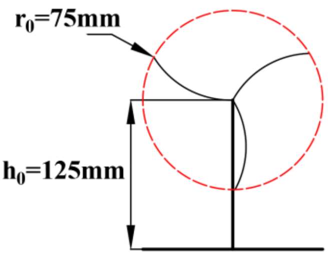

Figure 2 Turbine dimensions

In the experiments, the tip speed ratio was set as roughly 4 for the first row of WTs ($\lambda = 2\pi r\Omega/[60U_{hub}]$, where U_{hub} was 2.1 m/s and Ω is the angular speed of the WT in r.p.m.).

4.2 Description of the incoming wind

To simulate the incoming wind of the experiments, equation (4) is adopted. To begin with, a vertical velocity profile was selected to see the accuracy of the 3-D single wake model, of which the position was at downstream distance of $x/D = 2$ behind the third row of WTs [30]. The simulations of this study are compared to the measured data, as shown in Figure 3. In this process, the power law parameter of wind speed was set as $\alpha = 0.1$.

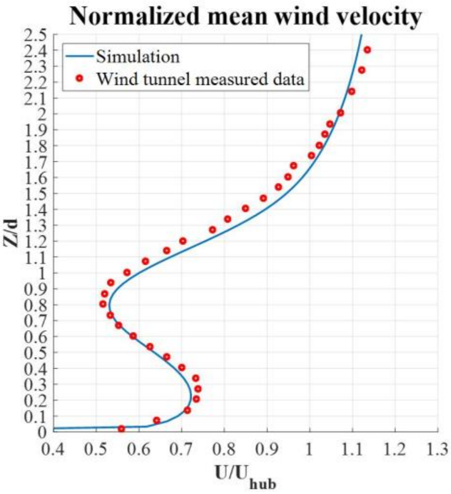

Figure 3   Distribution of the normalized streamwise velocity component

The simulation results show a perfect agreement with the measured data, especially at the hub height. The deficit in the wind farm is also given in reference [30]. Combining the streamwise wind velocity and the wind deficit, the recovery data incoming wind in the wind tunnel can also be obtained. Then, the recovery data are compared with the simulation results, as shown in Figure 4.

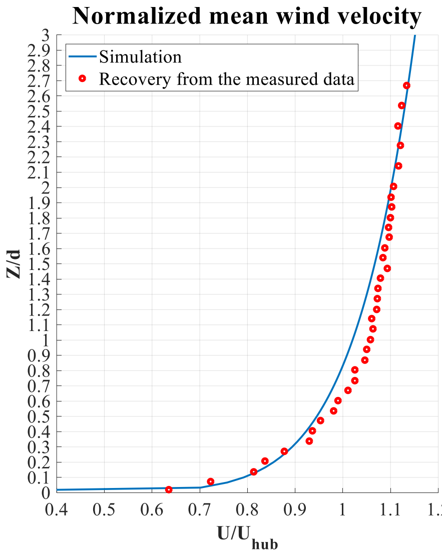

Figure 4   Incoming wind distribution

Error comparisons could be done between the simulation results and the measured data through Figure 4. Generally, the simulated incoming wind speeds fit well with the experimental data. Some big errors exist in the height range of 0.5D ~1.5D (D represents the rotor diameter of the wind turbine). It is worthy noticing that these errors may have an influence on the validation of the effectiveness of the 3-D multiple wake model.

4.3 Results comparison

The comparisons have been carried out with the experiments of two layouts, which are both the 10 by 3 WT arrays.

4.3.1 Results comparison of Layout 1

In Layout 1, the distance between consecutive WTs was set to 5D in the direction of the inflow and 4D in the spanwise direction. The schematic WT array is demonstrated in Figure 5.

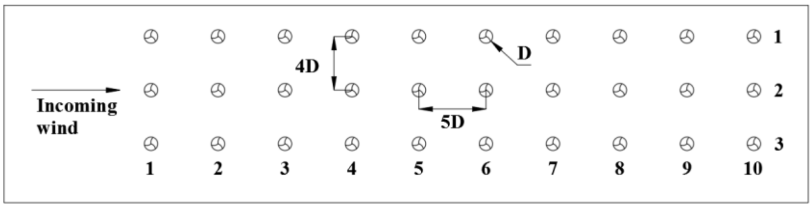

Figure 5 Schematic wind turbine array

Figure 6 shows the simulation results of the 3-D wake model in Layout 1. The results are compared to the representative wind speeds measured in the wind tunnel experiment at three heights: (a) the bottom tip height; (b) the hub height; and (c) the top tip height.

(a)

(b)

(c)

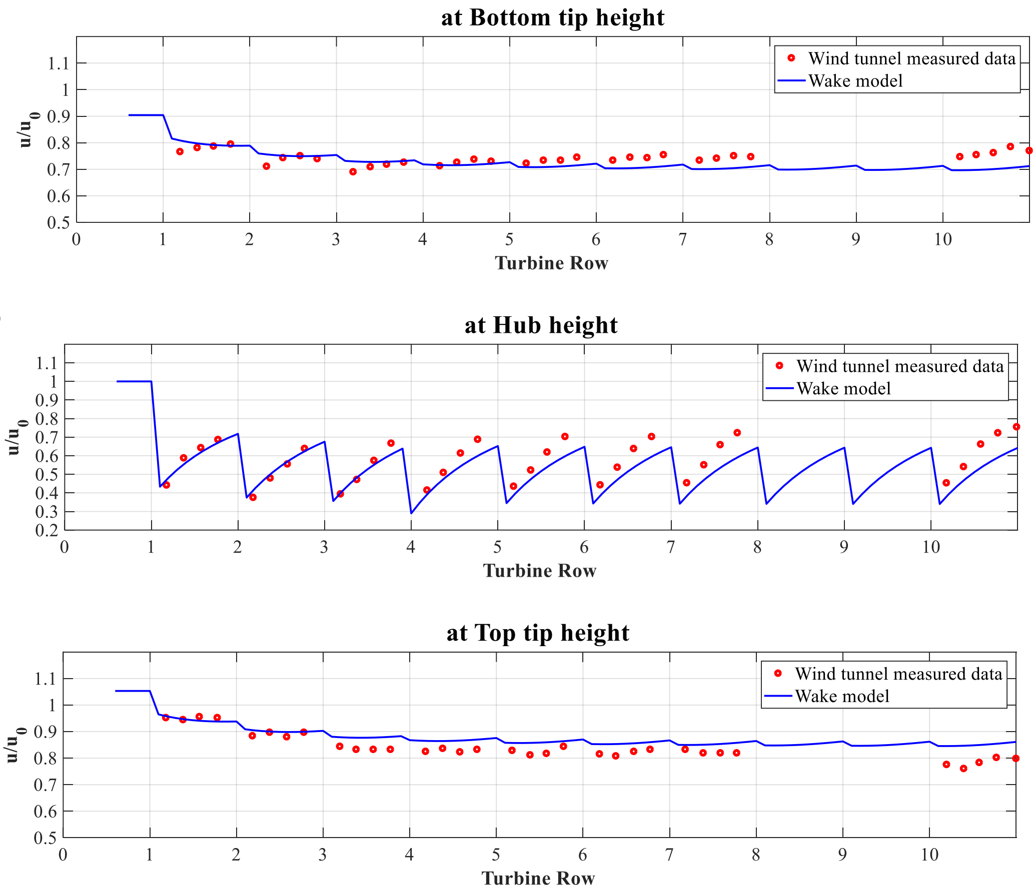

Figure 6 Comparison wind speeds at (a) the bottom tip height; (b) the hub height; and (c) the top tip height.

At all three representative heights, the 3-D multiple wake model tends to predict wind speed distribution accurately. For the first two rows, the prediction results are very close to the measured data. For the rest rows, although some deviations exist, the shapes of the predictions and the characterizations of the mean flow are in good accordance at all heights. The 3-D wake model tends to predict smaller wind speeds at the bottom tip and the hub heights after the 4th row, while predict larger wind speeds at the top tip height after the 3rd row.

Apart from the errors from the wake model, some errors may also come from the experiment. Taking the hub height data as an example, the wind speeds measured at the downwind behind rows tend to be larger than those at the front rows, which is not quite rational. The experimental errors should be involved in the consideration when judging the effectiveness of the 3-D multiple wake model.

The relative errors at three heights of Layout 1 are then analyzed and demonstrated in Figure 7.

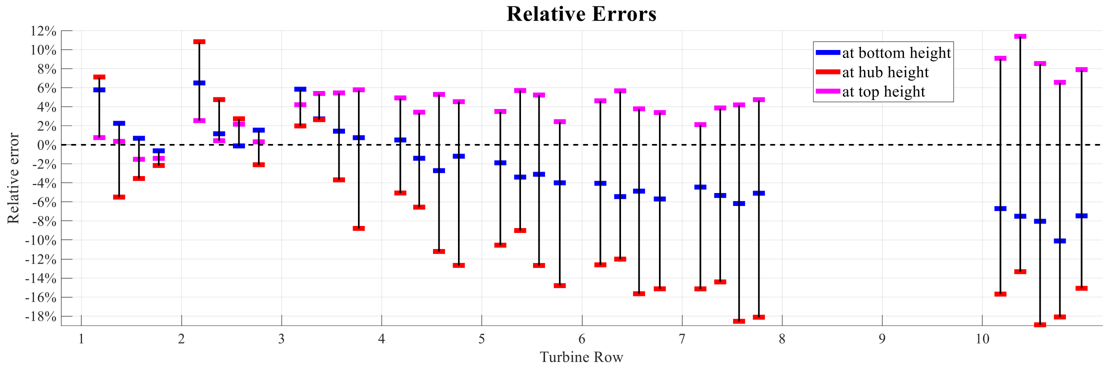

Figure 7 Analysis of relative errors of Layout 1

It is apparent that the simulation from the wake model is more precise at the hub and the top heights, where most of the relative errors are smaller than 6%. The wake model does not seem to be that accurate at the top height, but all relative errors are within 20%. The similar conclusion can be obtained that the wake model predicts better in the first three rows than in the rest behind rows.

4.3.2 Results comparison of Layout 2

In Layout 2, the interval in the spanwise direction was also 4D, but that in the downwind direction was 7D. The schematic WT array is demonstrated in Figure 8.

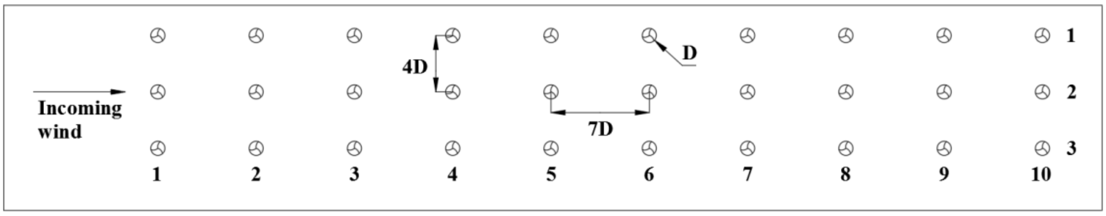

Figure 8 Schematic of wind turbine array with 10 lines and 3 rows

Figure 9 demonstrates the simulation results of the 3-D wake model in Layout 2. They are also compared with the wind speeds measured from the wind tunnel experiment. The three representative positions are: (a) the bottom tip height; (b) the hub height; and (c) the top tip height.

(a)

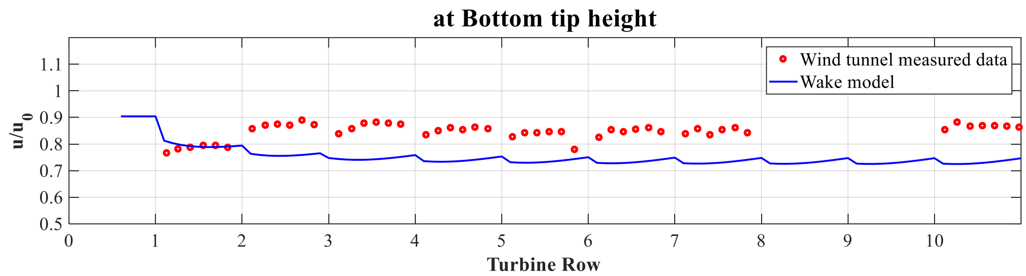

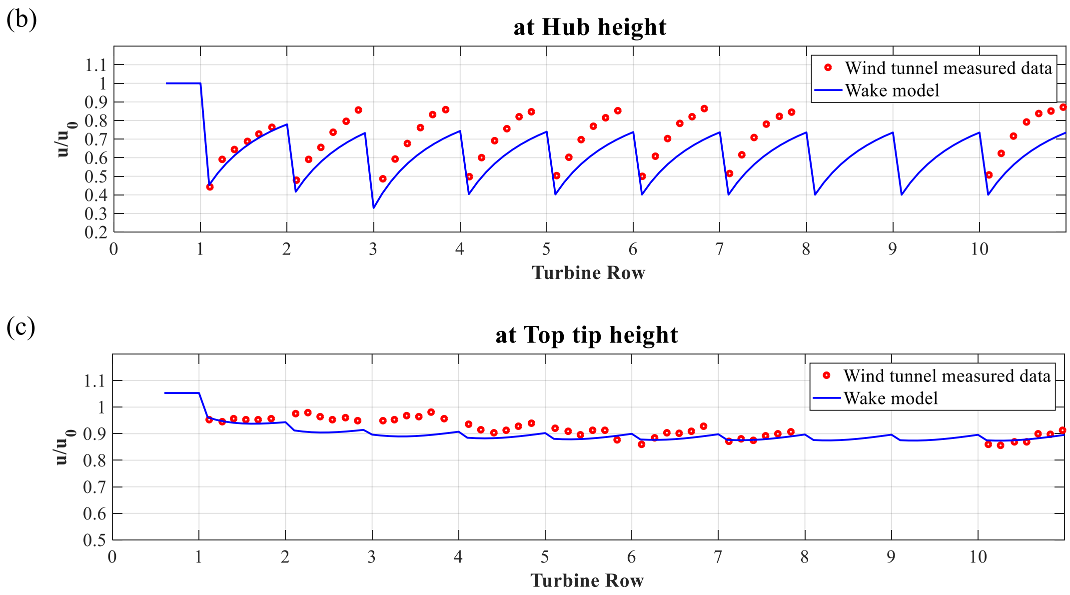

Figure 9 Comparison wind speeds at (a) the bottom tip height; (b) the hub height; and (c) the top tip height.

For Layout 2, the 3-D wake model also shows the good accuracy. It tends to underestimate the wind speed at all selected heights. Good agreement between the simulated results and the experimental data is shown at the space between the 1st and the 2nd rows. The wake model is especially precise at the top tip height. For the bottom tip and the hub heights, an obvious difference lies between the measured wind speeds of the 1st row and the 2nd row, which may affect the validation of the 3-D wake model. Therefore, some more comprehensive wind tunnel tests should be conducted in the future research to investigate this 3-D wake model.

The quantitative analysis of relative errors is revealed in Figure 10.

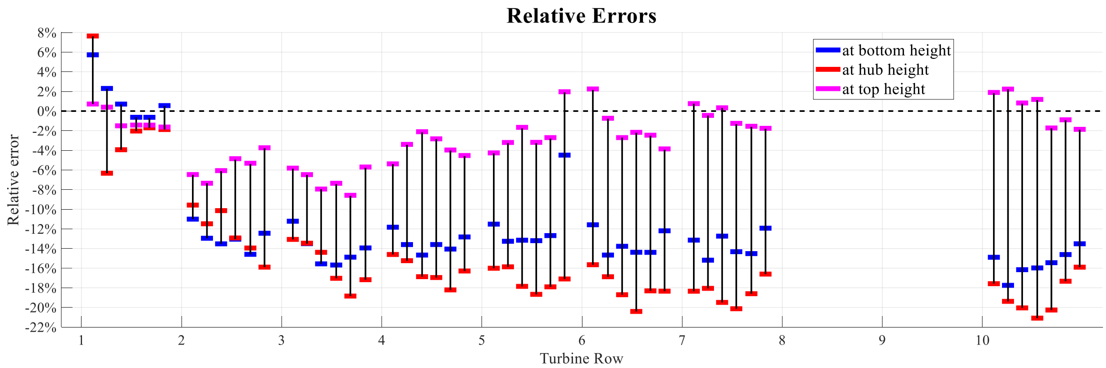

Figure 10 Analysis of relative errors in Layout 2

From the figure, for Layout 2, the 3-D wake model simulates the wake effect with an acceptable precision, and the largest error is smaller than 22%. The model is more precise before the 2nd row. It is most accurate at the top height, followed by the bottom height and the hub height. At the top height, the largest error is just 8.5%, those at the bottom and the hub heights are 17.8% and 21.2%, respectively.

The 3-D WT wake model tends to underestimate wind speed in some positions. On the one hand, when derivating the wake model, a modification was made from equation (14) to equation (15). Although it is reasonable according to the reference [29], it may cause the error to the 3-D wake model. On the other hand, as analyzed before, some measuring data seem to contain the experimental errors, which means the experimental error may affect the validation of the 3-D wake model. Therefore, the 3-D wake model can be further improved and the more accurate wind tunnel experiments should be conducted.

5. Prediction of the three-dimensional multiple wake model

After validating the accuracy of the 3-D multiple wake model, some predictions of wake distribution can be obtained. In this chapter, the model is used to simulate the wind speed profiles in the mentioned two layouts from some more views.

5.1 Prediction of Layout 1

In this section, the simulated layout of wind farm is the same as Layout 1. Three different views are demonstrated. Figure 11 is the X-Z view of wind speed at Y=0D.

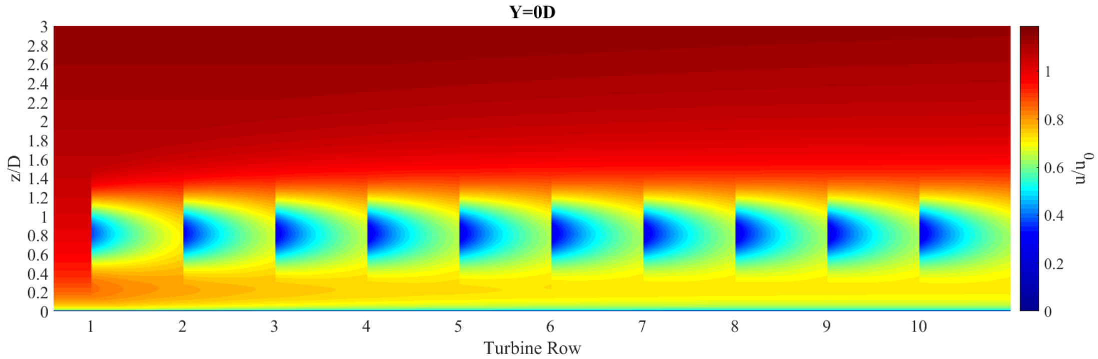

Figure 11 X-Z view of wind speed at Y=0D.

The wake distributions vary in the downstream direction, which can be seen from Figure 11. The wind deficit behind the 1st row of WT is the smallest. With the wind blowing through WTs, the wind deficit phenomenon becomes more obvious. Beyond the 5th row, the wind profiles behind each WTs seem to be pretty similar. According to Figure 11, the downstream intervals between WTs are recommended to be no less than 5D. For each vertical section, the largest wind deficit happens at the hub height. That is to say if the hub heights of WTs are different, the serious wake-influenced zone can be avoided, and more wind energy can be captured.

Figure 12 shows the X-Y view of wind velocity at the position where $Z = \text{hub height}$.

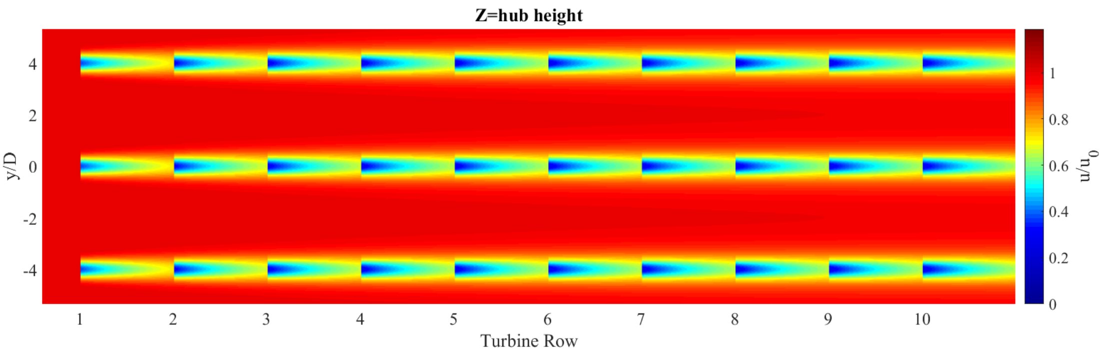

Figure 12 X-Y view of wind speed where $Z = \text{hub height}$.

The 3-D wake model helps to study the X-Y view of wind velocity at all heights. The largest deficit of wind happens at the hub height. From the figure, the 4D cross interval between WTs is long enough to avoid the wakes, because the parallel WTs almost have no influence to each other.

Figure 13 demonstrates the Y-Z view of wind speed at four typical X position: (a) X=1.2 Turbine Row;.(b) X=1.5 Turbine Row; (c) X=6.2 Turbine Row and (d) X=10.5 Turbine Row.

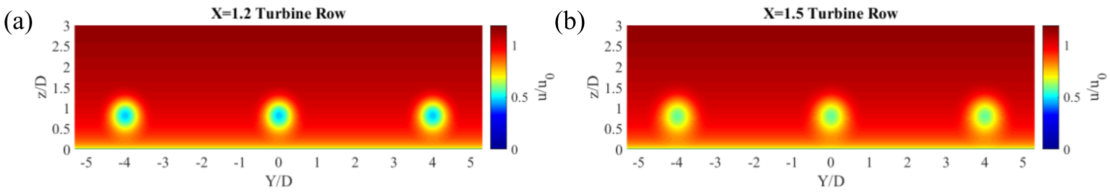

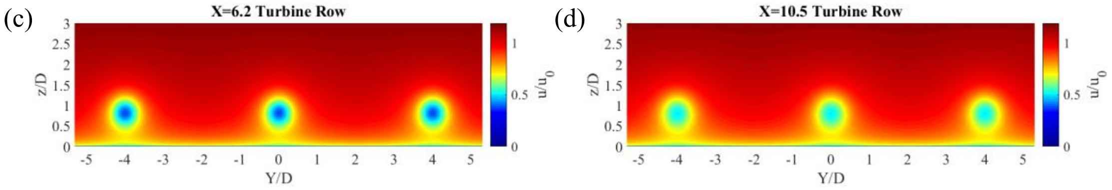

Figure 13 Y-Z view of wind speed at (a) X=1.2 Turbine Row;.(b) X=1.5 Turbine Row; (c) X=6.2 Turbine Row and (d) X=10.5 Turbine Row.

Comparing Figure 13 (a) and (c), the selected sections are at the same distance from the upwind WTs, however, the distributions of the wind speeds are much different. The reason is that the incoming wind for the 1st row of WTs is the environmental wind, which is not influenced by the wake of other WTs; whereas the incoming wind for the 6th row of WTs is smaller the environmental wind speed, as it is under the wake effect of other upstream WTs. It can also explain the difference between Figure 13 (b) and (d).

5.2 Prediction of Layout 2

This section is continuous to section 5.1, and the simulated layout of wind farm is the same as Layout 2. Firstly, Figure 14 shows the X-Z view of wind speed at Y=0D.

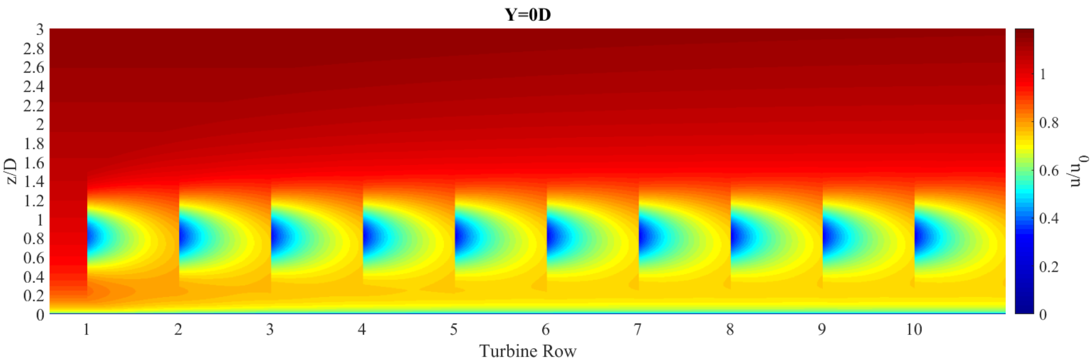

Figure 14 X-Z view of wind speed at Y=0D

The wind deficit behind the 1st row of WT is also the smallest, which is similar to that of Layout 1. The little difference is that after the 3rd row, wind profile behind each WT becomes similar. This is directly caused by the increase of intervals between the downwind WTs. Intervals of 7D distance tend to be better than 5D, as the downstream WTs are less influenced by the upstream WTs.

Figure 15 shows the X-Y view of wind speed at Z=hub height of Layout 2.

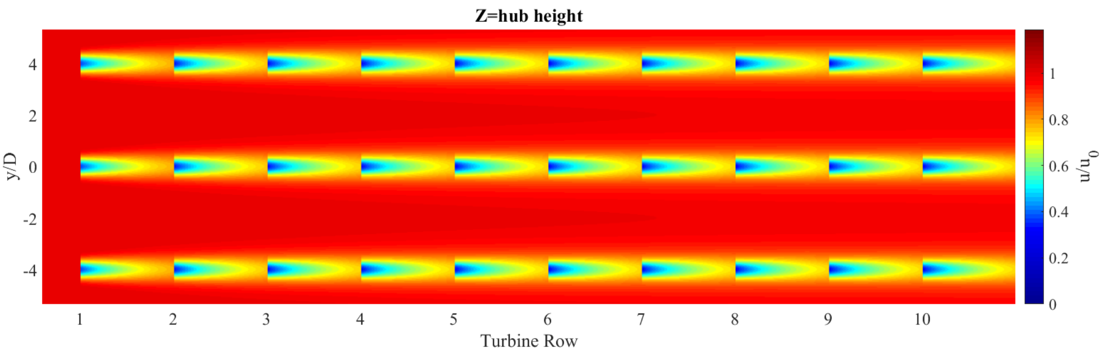

Figure 15 X-Y view of wind speed at $Z =$ hub height

This figure further confirms that Layout 2 is more efficient. The wake-influenced winds firstly blow through the upstream WTs and then recover to the environmental winds before reaching the downstream

WTs. If the intervals continue increasing, the downstream WTs can operate under less wake effect.

Figure 16 demonstrates the Y-Z view of wind speed at four typical X position: (a) X=1.2 Turbine Row; (b) X=1.5 Turbine Row; (c) X=6.2 Turbine Row and (d) X=10.5 Turbine Row. These profiles help to further investigate the characteristics of the WT wake effect.

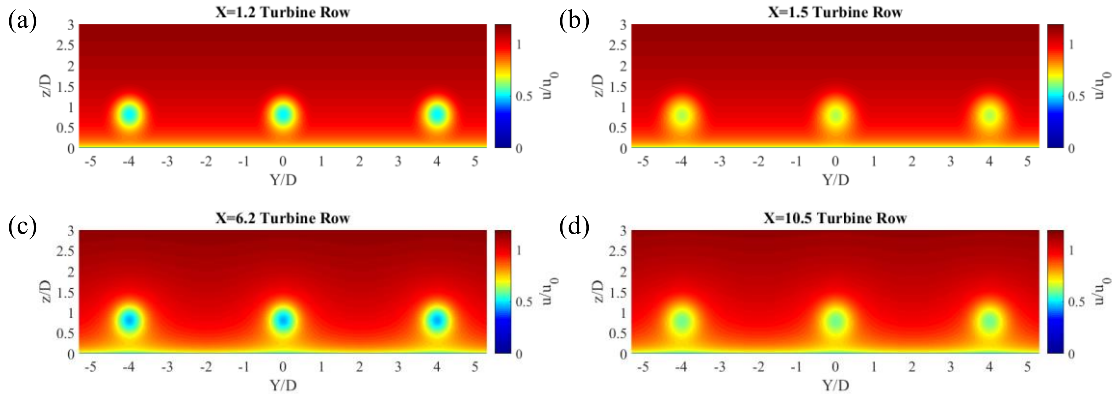

Figure 16 Y-Z view of wind speed at (a) $X = 1.2$ Turbine Row ; (b) $X = 1.5$ Turbine Row ; (c) $X = 6.2$ Turbine Row and (d) $X = 10.5$ Turbine Row

6. Summaries

In this study, an analytical three-dimensional (3-D) wake model has been further studied. The method to calculate the average wind speed of a single wind turbine is proposed, in which the wind variation in the vertical direction is considered. Then, the 3-D wake model for multiple wind turbines is developed. The significant summaries are drawn as follows:

(1) The average wind speed of a single wind turbine (WT) is studied in depth. The power law wind profile in 3-D wake model is adopted. The basic theory is the flow flux conservation law. From the results, under the condition of the mentioned incoming wind profile, the average wind velocity of a wind turbine is smaller than the wind velocity measured at the hub height. For the same power exponent α, the average wind speed increases with the hub height but decreases with the rotor radius. The power exponent α also influences the average wind speed. To be specific, the deficit of wind speed increases with α. When $\alpha = 0.1$, the average wind speed is reduced by 2% to the most, whereas when $\alpha = 0.4$, the average wind speed can decrease by 4%. Therefore, the reduction of average wind speed should be considered especially for wind turbines that have large rotor radius, stand at high positions and are built in terrains with large irregular objects.

(2) The 3-D wake model for multiple wind turbines was derived. The single wake model was rewritten in the global coordinate. Sum of Squares method was adopted to solve the wake adding problem accordingly. If the WT_i has been judged to be affected by the wake effect of other n WTs, the formula can be further specified as:

$$U_i(x,y,z) = U_0(z) - \sqrt{\sum_{j=1}^{n}[A_j(x)(\frac{1}{2\pi\sigma_j(x)^2}e^{-\frac{(y-y_j)^2+(z-h_0)^2}{2\sigma_j(x)^2}}) + B_j(x)]^2}$$

(3) The 3-D multiple wake model has been validated by the wind tunnel experimental data of two layouts of miniature WTs. In Layout 1, the wake model was pretty accurate at the hub and the top heights, and most of the relative errors were smaller than 6%. At the top height, all relative errors were smaller 20%. The wake model predicted more precise for the first three rows than the rest rows. In Layout 2, the wake model also predicted the wake effect with acceptable precisions, and the largest error was smaller than 22%. The model was more accurate within the first-row distance. At the top height, the largest error of the wake model was just 8.5%, which was 17.8% at the bottom height and 21.2% at the hub height.

(4) Some wind predictions of the mentioned two layouts of the miniature WTs were obtained from the 3-D wake model. The profiles of wind speeds from some more views were demonstrated. From the predicted results, the largest wind deficit was at the hub height and the 4D cross interval between WTs was large enough to avoid the serious wake effect. Comparing two layouts, intervals of 7D distance were better than 5D, as the downstream WTs were almost unaffected by the upwind WTs.

This study has assessed the feasibility of applying the 3-D multiple wake model to estimate the deficits of wind speeds. The wake model takes the vertical wind variation into consideration, which potentially contributes to optimizing the heights of WTs and helps to design the layout of the nonuniform wind farm that contains different sizes of WTs. The presented wake model also has some limitations, thus some further research should be conducted in the future. In this study, the power function was adopted to simulate the incoming wind, some errors were found between the simulation and experimental data, which may bring errors to the final predictions of the downstream wind speeds. The power function cannot predict some complicate wind profiles in the real wind industry and it increases the complexity of the calculation as well. Therefore, it is necessary to adopt a more precise and simpler function to take place of the present power function. The published wind tunnel experimental data are not quite enough to continue an in-depth investigation of the presented wake model. Well-directed wind field experiments and wind tunnel tests should be conducted to investigate and complete the 3-D wind turbine wake model in the future work.

Acknowledgement

The work described in this paper was supported by the Research Institute for Sustainable Urban Development (RISUD) with account number of BBW8 and the FCE Dean Research project with account number of ZVHL, The Hong Kong Polytechnic University.

References

[1] W. Tong, S. Chowdhury, J. Zhang, and A. Messac, "Impact of different wake models on the estimation of wind farm power generation," in *12th AIAA Aviation Technology, Integration, and Operations (ATIO) Conference and 14th AIAA/ISSMO Multidisciplinary Analysis and Optimization Conference*, 2012, p. 5430.

[2] J. Schmidt and B. Stoevesandt, "The impact of wake models on wind farm layout optimization," in *Journal of Physics: Conference Series*, 2015, vol. 625, no. 1, p. 012040: IOP Publishing.

[3] T. Ishihara, A. Yamaguchi, and Y. Fujino, "Development of a new wake model based on a wind tunnel experiment," *Global wind power,* vol. 6, 2004.

[4] N. O. Jensen, *A note on wind generator interaction*. 1983.

[5] G. C. Larsen, "A simple stationary semi-analytical wake model," Risø National Laboratory for Sustainable Energy, Technical University of Denmark2009.

[6] J. Kuo, D. Rehman, D. A. Romero, and C. H. Amon, "A novel wake model for wind farm design on complex terrains," *Journal of Wind Engineering and Industrial Aerodynamics,* vol. 174, pp. 94-102, 3// 2018.

[7] M. X. Song, B. H. Wu, K. Chen, X. Zhang, and J. Wang, "Simulating the wake flow effect of wind turbines on velocity and turbulence using particle random walk method," *Energy,* vol. 116, pp. 583-591, Dec 2016.

[8] L. P. Chamorro and F. Porté-Agel, "A wind-tunnel investigation of wind-turbine wakes: boundary-layer turbulence effects," *Boundary-layer meteorology,* vol. 132, no. 1, pp. 129-149, 2009.

[9] N. P. Dufresne and M. Wosnik, "Velocity deficit and swirl in the turbulent wake of a wind turbine," *Marine Technology Society Journal,* vol. 47, no. 4, pp. 193-205, 2013.

[10] M. Bastankhah and F. Porté-Agel, "A new analytical model for wind-turbine wakes," *Renewable Energy,* vol. 70, pp. 116-123, 10// 2014.

[11] L. L. Tian, W. J. Zhu, W. Z. Shen, N. Zhao, and Z. W. Shen, "Development and validation of a new two-dimensional wake model for wind turbine wakes," *Journal of Wind Engineering and Industrial Aerodynamics,* vol. 137, pp. 90-99, Feb 2015.

[12] X. Gao, H. Yang, and L. Lu, "Optimization of wind turbine layout position in a wind farm using a newly-developed two-dimensional wake model," *Applied Energy,* vol. 174, pp. 192-200, 2016.

[13] H. Sun and H. Yang, "Study on an innovative three-dimensional wind turbine wake model," *Applied Energy,* vol. 226, pp. 483-493, 2018/09/15/ 2018.

[14] H. Sun, H. Yang, and X. Gao, "Investigation into spacing restriction and layout optimization of wind farm with multiple types of wind turbines," *Energy,* vol. 168, pp. 637-650, 2019/02/01/ 2019.

[15] A. Jimenez, A. Crespo, E. Migoya, and J. García, "Advances in large-eddy simulation of a wind turbine wake," in *Journal of Physics: Conference Series*, 2007, vol. 75, no. 1, p. 012041: IOP Publishing.

[16] Y.-T. Wu and F. Porté-Agel, "Large-eddy simulation of wind-turbine wakes: evaluation of turbine parametrisations," *Boundary-layer meteorology,* vol. 138, no. 3, pp. 345-366, 2011.

[17] X. Yang and F. Sotiropoulos, "On the predictive capabilities of LES-actuator disk model in simulating turbulence past wind turbines and farms," in *American Control Conference (ACC), 2013*, 2013, pp. 2878-2883: IEEE.

[18] N. Sedaghatizadeh, M. Arjomandi, R. Kelso, B. Cazzolato, and M. H. Ghayesh, "Modelling of wind turbine wake using large eddy simulation," *Renewable Energy,* vol. 115, pp. 1166-1176, 1// 2018.

[19] L. P. Chamorro, R. Arndt, and F. Sotiropoulos, "Turbulent flow properties around a staggered wind farm," *Boundary-layer meteorology,* vol. 141, no. 3, pp. 349-367, 2011.

[20] W. Tian, A. Ozbay, and H. Hu, "An experimental study on the effects of incoming wind conditions on wind turbine aeromechanics," 2014.

[21] N. Wildmann, S. Kigle, and T. Gerz, "Coplanar lidar measurement of a single wind energy converter wake in distinct atmospheric stability regimes at the Perdigao 2017 experiment," in *Journal of Physics: Conference Series*, 2018, vol. 1037.

[22] X. Gao, H. Yang, and L. Lu, "Study on offshore wind power potential and wind farm optimization in Hong Kong," *Applied Energy,* vol. 130, pp. 519-531, 2014.

[23] L. Lu, H. Yang, and J. Burnett, "Investigation on wind power potential on Hong Kong islands—an analysis of wind power and wind turbine characteristics," *Renewable Energy,* vol. 27, no. 1, pp. 1-12, 9// 2002.

[24] E. W. Peterson and J. P. Hennessey Jr, "On the use of power laws for estimates of wind power potential," *Journal of Applied Meteorology,* vol. 17, no. 3, pp. 390-394, 1978.

[25] Wikipedia. *Wind profile power law*. Available: https://en.wikipedia.org/wiki/Wind_profile_power_law

[26] H. Dobesch and G. Kury, *Basic meteorological concepts and recommendations for the exploitation of wind energy in the atmospheric boundary layer*. Zentralanstalt für Meteorologie und Geodynamik, 2006.

[27] D. J. Renkema, "Validation of wind turbine wake models," Master of Science, Faculty of Aerospace Engineering, Delft University of Technology, 2007.

[28] E. Djerf and H. Mattsson, "Evaluation of the software program windfarm and comparisons with measured data from alsvik," *The aeronautical research institute of Sweden,* 2000.

[29] B. Lange, H. P. Waldl, A. G. Guerrero, D. Heinemann, and R. J. Barthelmie, "Modelling of offshore wind turbine wakes with the wind farm program FLaP," *Wind Energy,* vol. 6, no. 1, pp. 87-104, 2003.

[30] L. P. Chamorro and F. Porte-Agel, "Turbulent Flow Inside and Above a Wind Farm: A Wind-Tunnel Study," *Energies,* vol. 4, no. 11, pp. 1916-1936, Nov 2011.

[31] M. A. Carper and F. Porté-Agel, "Subfilter-scale fluxes over a surface roughness transition. Part I: Measured fluxes and energy transfer rates," *Boundary-layer meteorology,* vol. 126, no. 1, pp. 157-179, 2008.

[32] M. A. Carper and F. Porté-Agel, "Subfilter-scale fluxes over a surface roughness transition. Part II: A priori study of large-Eddy simulation models," *Boundary-layer meteorology,* vol. 127, no. 1, pp. 73-95, 2008.